

Strathprints Institutional Repository

Liu, Tung-Chang and Shao, Xi and Liu, Chuan-Sheng and Su, Jao-Jang and Eliasson, Bengt and Tripathi, Vipin and Dudnikova, Galina and Sagdeev, Roald Z. (2011) *Energetics and energy scaling of quasi-monoenergetic protons in laser radiation pressure acceleration*. *Physics of Plasmas*, 18 (12). ISSN 1070-664X

Strathprints is designed to allow users to access the research output of the University of Strathclyde. Copyright © and Moral Rights for the papers on this site are retained by the individual authors and/or other copyright owners. You may not engage in further distribution of the material for any profitmaking activities or any commercial gain. You may freely distribute both the url (<http://strathprints.strath.ac.uk/>) and the content of this paper for research or study, educational, or not-for-profit purposes without prior permission or charge.

Any correspondence concerning this service should be sent to Strathprints administrator: <mailto:strathprints@strath.ac.uk>

Energetics and energy scaling of quasi-monoenergetic protons in laser radiation pressure acceleration

Tung-Chang Liu, Xi Shao, Chuan-Sheng Liu, Jao-Jang Su, Bengt Eliasson et al.

Citation: *Phys. Plasmas* **18**, 123105 (2011); doi: 10.1063/1.3672515

View online: <http://dx.doi.org/10.1063/1.3672515>

View Table of Contents: <http://pop.aip.org/resource/1/PHPAEN/v18/i12>

Published by the AIP Publishing LLC.

Additional information on Phys. Plasmas

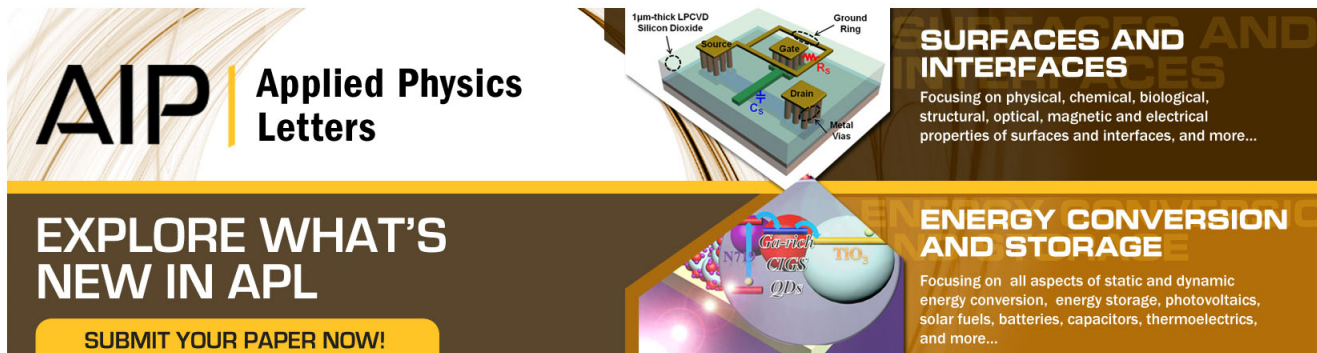
Journal Homepage: <http://pop.aip.org/>

Journal Information: http://pop.aip.org/about/about_the_journal

Top downloads: http://pop.aip.org/features/most_downloaded

Information for Authors: <http://pop.aip.org/authors>

ADVERTISEMENT



AIP | Applied Physics Letters

SURFACES AND INTERFACES
Focusing on physical, chemical, biological, structural, optical, magnetic and electrical properties of surfaces and interfaces, and more...

ENERGY CONVERSION AND STORAGE
Focusing on all aspects of static and dynamic energy conversion, energy storage, photovoltaics, solar fuels, batteries, capacitors, thermoelectrics, and more...

EXPLORE WHAT'S NEW IN APL

SUBMIT YOUR PAPER NOW!

Labels in the 3D schematic: 1µm-thick LPCVD Silicon Dioxide, Source, Gate, Drain, Metal Vias, Ground Ring, Cs, R_s.

Labels in the energy conversion diagram: QDs, CIGS, NTG, NO₂.

Energetics and energy scaling of quasi-monoenergetic protons in laser radiation pressure acceleration

Tung-Chang Liu,¹ Xi Shao,¹ Chuan-Sheng Liu,¹ Jao-Jang Su,¹ Bengt Eliasson,^{1,2} Vipin Tripathi,³ Galina Dudnikova,¹ and Roald Z. Sagdeev¹

¹University of Maryland, College Park, Maryland 20742, USA

²Ruhr-University Bochum, D-44780 Bochum, Germany

³Indian Institute of Technology, New Delhi 110016, India

(Received 18 August 2011; accepted 17 November 2011; published online 29 December 2011)

Theoretical and computational studies of the ion energy scaling of the radiation pressure acceleration of an ultra-thin foil by short pulse intense laser irradiation are presented. To obtain a quasi-monoenergetic ion beam with an energy spread of less than 20%, two-dimensional particle-in-cell simulations show that the maximum energy of the quasi-monoenergetic ion beam is limited by self-induced transparency at the density minima caused by the Rayleigh-Taylor instability. For foils of optimal thickness, the time over which Rayleigh-Taylor instability fully develops and transparency occurs is almost independent of the laser amplitude. With a laser power of about one petawatt, quasi-monoenergetic protons with 200 MeV and carbon ions with 100 MeV per nucleon can be obtained, suitable for particle therapy applications. © 2011 American Institute of Physics. [doi:10.1063/1.3672515]

I. INTRODUCTION

Successful experimental demonstrations of laser-plasma wake-field acceleration in the bubble regime of high quality, quasi-monoenergetic electron beams up to 1 GeV (Refs. 1 and 2) have generated considerable interest in the development of compact charged particle accelerators with a wide range of potential applications. It is, therefore, timely to investigate the feasibility of laser acceleration of quasi-monoenergetic hadrons, which can have tremendous beneficial applications such as particle therapy for cancer treatment,³ fast ignition,^{4,5} and proton imaging methods.^{6,7} Indeed, there has been considerable interest in laser hadron accelerator studies, with the advent of short pulse intense lasers with wavelengths of about one micron and intensities of about 10^{20} W/cm². In early studies of laser acceleration of highly energetic ions, thick foil targets with thicknesses ranging from a few to tens of laser wavelengths were employed and the target normal sheath acceleration (TNSA) was the predominant mechanism leading to the production of multi-tens MeV ion beams.^{8–16} The resulting ion energy spectrum, however, is broad and only a small fraction of the protons reach the maximum energy, which is less than 67 MeV thus far,¹⁷ not suitable for applications requiring high quality beams of monoenergetic ions.

Recently, a scheme of laser radiation pressure acceleration (RPA) of an ultra-thin target, where a self-organized double layer plasma is accelerated by reflecting the laser, was considered an efficient way of accelerating quasi-monoenergetic ions.^{18–26} In comparison to the conventional TNSA-scheme,¹² the conversion efficiency with the RPA scheme is estimated to be more than 40 times higher. Recent simulations of the RPA scheme focused on case studies of obtaining GeV protons with high power (about tens of petawatt) laser irradiated on single species ion target.^{27,28} Using a 30 TW laser with a peak intensity of 5×10^{19} W/cm² irradiated on a diamond-like carbon (DLC) foil of thickness

5.3 nm, Henig *et al.* obtained a C⁶⁺ ion beam with a distinct peak energy of around 30 MeV and an energy spread of around 20 MeV by both 2D simulations and experiments.²⁹ In this paper, we address factors limiting the energy of RPA accelerated ions and the energy scaling of quasi-monoenergetic ions as a function of the laser power. Both questions are important for theoretical understanding, experimental planning, and future applications.

In RPA, high intensity circularly polarized laser with high contrast ratio accelerates the ultra-thin foil by the ponderomotive force acting on the electrons.²² The laser sweeps all electrons in the foil forward until the electrostatic force due to the ions left behind balances the ponderomotive force at a distance D . When the thickness of the target l_0 is equal to D , we obtain optimal thickness. In the limit of normalized laser amplitude $a_0 = e|E_0|/(m\omega_L c) \gg 1$, this thickness is²²

$$l_0 \approx \frac{4\pi}{\lambda_L} \left(\frac{c}{\omega_p} \right)^2 a_0 = \frac{\lambda_L}{\pi} \left(\frac{\omega_L}{\omega_p} \right)^2 a_0 = \frac{a_0 n_c}{\pi n_0} \lambda_L, \quad (1)$$

where m and $-e$ are the electron mass and charge, λ_L and ω_L are the laser wavelength and angular frequency, ω_p is the electron plasma frequency, n_0 is the target electron density, and $n_c = \epsilon_0 m \omega_L^2 / e^2$ is the critical density. To minimize the wave tunneling through the target, $l_0 > c/\omega_p$ or equivalently $2a_0 \omega_L / \omega_p > 1$ should be satisfied. In RPA, the ions are accelerated forward by the electric force of the electron layer and the inertial force in the accelerating frame moving with the foil pulls them back. The balance of these two opposing forces forms a trap for the ions in real and phase spaces. These stably trapped ion and electron layers form a self-organized double layer in one dimension, accelerated as a whole by the laser radiation pressure, and the ions thus accelerated are nearly monoenergetic. The equation of motion for the foil in one dimension, based on energy conservation,²² is

$$\frac{d(\gamma\beta)}{dt} = \frac{2I_0}{m_i n_0 l_0 c^2} \frac{1 - \beta}{1 + \beta}, \quad (2)$$

where $\gamma = (1 - \beta^2)^{-1/2}$, $\beta = v/c$ is the foil velocity, and $m_i n_0 l_0$ is the mass of the double layer. Equation (2) can be analytically solved to obtain the ion kinetic energy $\varepsilon_i(t) = (\gamma - 1)m_i c^2$ and momentum $p_{ix} = \gamma\beta m_i c$. Theoretically, $\varepsilon_i(t) \rightarrow \infty$ as $t \rightarrow \infty$, that is, the foil could be unlimitedly accelerated as long as being impinged by the laser. However, the time for monoenergetic ion acceleration with RPA is limited by the duration in which the double layer can maintain its overdense properties, which can be lost due to the development of the Rayleigh-Taylor instability (RTI),^{24–26,30} which is one of the most important instabilities arising when a thin plasma foil is accelerated by the radiation pressure of an intense laser. It poses a limit on the time a foil can be accelerated before it loses its monoenergetic properties.

II. SIMULATION SETUP AND RESULTS

We here employ two-dimensional (2D) particle-in-cell (PIC) simulations to demonstrate the generation and energy scaling of quasi-monoenergetic ions by the RPA with laser radiation intensity.³¹ The simulation domain is $-4 \leq x/\lambda_L \leq 12$; $-12 \leq y/\lambda_L \leq 12$ and is divided into 64 grids per wavelength. The boundary condition is periodic in y direction and out flow in x direction. The foil is initially located at $0 \leq x \leq l_0$ with $l_0 = 0.2\lambda_L$ being the foil thickness and is resolved by about 10^6 quasi-particles of each species (protons and electrons). The time step is $0.0027T_L$, which is four times finer than the Courant–Friedrichs–Lewy condition, to avoid inaccuracy from simulation approximation and ensure that the results are a consequence of real physics, where $T_L = 3.33$ fs is the laser period, corresponding to $\lambda_L = 1\mu\text{m}$. The amplitude of the incident circularly polarized laser has a Gaussian profile in the transverse direction with the spot size being $16\lambda_L$ in diameter and a trapezoidal time

profile with $3T_L$ rising, $24T_L$ flat, and $3T_L$ falling time, respectively.

Figure 1 shows 2D PIC simulation results of the RPA of a thin foil with a normalized incident laser amplitude, $a_0 = 25$, initial foil density, $n_0 = 41.7n_c$, and foil thickness, $l_0 = 0.2\lambda_L$ corresponding to the optimal thickness as defined in Eq. (1). It shows that the RTI can destroy the electron layer and widen the energy spectrum of the ions. For effective acceleration and production of monoenergetic particles, it is important to maintain the target density as over-dense, i.e., $n \geq \gamma_e n_c$, where $\gamma_e = (1 - v_e^2/c^2)^{-1/2}$ provides the relativistic correction and $n_c = \varepsilon_0 m_e \omega_L^2 / e^2$ is the non-relativistic critical density. For the electron layer driven by laser light, γ_e within the laser penetration depth will be approximately equal to a_0 for $a_0 \gg 1$, so the relativistic critical density can be approximated as $n_c a_0$. During the linear phase of the RTI, small perturbations, or ripples, on the surface of the foil grow exponentially. These perturbations will grow into large amplitude periodic structures and form interleaving high density blobs and low density regions for both the electron and ion layers, as shown in Fig. 1. Figure 1 also shows that the transverse wavelength of the periodical structure is comparable to the laser wavelength. The density difference between the high and low density regions can grow very rapidly and filaments, or fingerlike structures, can be further developed. Once the density of the low density region of the foil falls below the critical value (evolution shown in the third column in Fig. 1, the laser light can penetrate that region (the fifth column in Fig. 1), after which the energy cannot be converted into foil acceleration efficiently, and the particle energy spread will be significantly increased (the sixth column in Fig. 1) due to laser-induced heating and Coulomb explosion. This leads to a leakage of radiation through the target by self-induced transparency. After this stage, the foil can no longer be accelerated efficiently and the energy spectrum starts to broaden dramatically and thus loses its monoenergetic property.

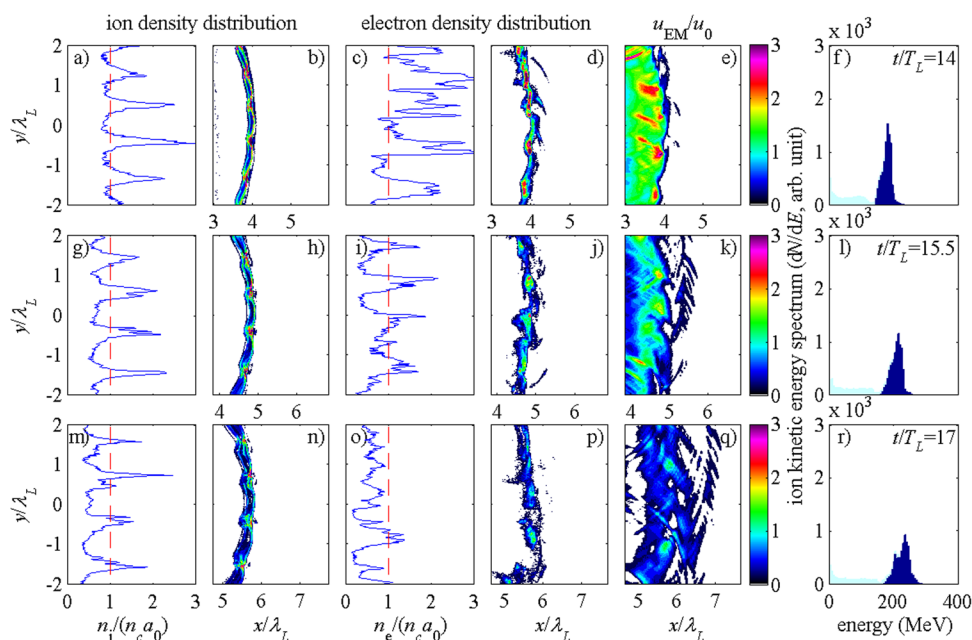


FIG. 1. (Color online) 2D PIC simulation results of the evolution of averaged proton density transverse to laser beam (the first column), proton density map (the second column), averaged electron density transverse to laser beam (the third column), electron density map (the fourth column), normalized electromagnetic field energy density over incident laser energy density (the fifth column), and energy spectrum of the protons (the sixth column) at three instants. Top, middle, and bottom rows are at $t = 14T_L$, $15.5T_L$, and $17T_L$, respectively. The vertical dashed lines show the critical density value. In the last column, dark-blue histograms in dark color show proton spectra collected within a window of $|y| < \lambda_L$ and a width of $\lambda_L/2$ in x co-moving with the foil; light-colored ones show proton spectra within $|y| < \lambda_L$ and covering the entire simulation range in x .

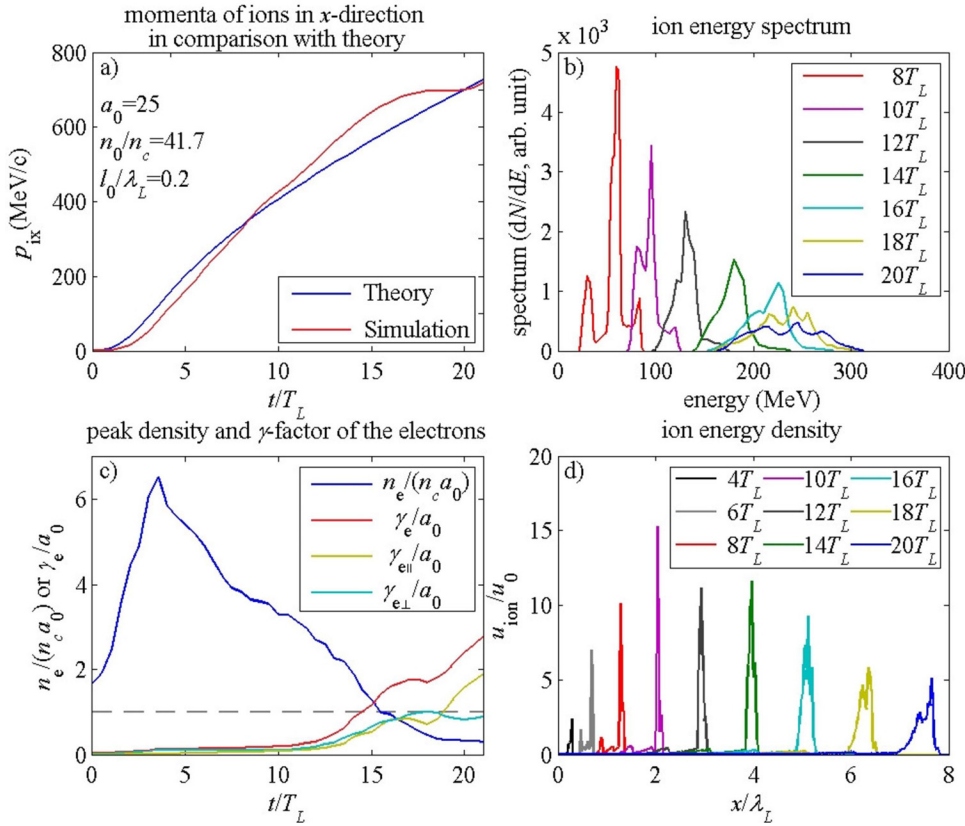


FIG. 2. (Color online) Simulation results with the same input parameters as in Fig. 1(a). Time evolution of ion momentum averaged within a $0.5\lambda_L \times 2\lambda_L$ window co-moving with the target from simulation (red line) and 1D theoretical calculation (blue line) using Eq. (2). (b) The evolution of ion energy spectra collected within the window as defined in (a). (c) The time evolution of normalized average density $n_e/(n_c a_0)$, of the electron layer (blue line), average γ_e/a_0 , $\gamma_{e\parallel}/a_0$, and $\gamma_{e\perp}/a_0$ within a $0.05\lambda_L \times 4\lambda_L$ window co-moving with the target. The time when $n_e/(n_c a_0) \approx 1$ is around $t = 16T_L$. (d) Evolution of the spatial distribution of the normalized ion energy density. The energy density is averaged over $1\lambda_L$ in y . The normalization factor $u_0 \approx 5.7 \times 10^{16} \text{J/m}^3$ is the incident laser energy density.

Figure 2(a) shows the general agreements between theory and simulation for the time evolution of the ion momentum p_{ix} averaged over a $0.5\lambda_L \times 2\lambda_L$ window co-moving with the target. The simulation shows slightly higher values of p_{ix} than the 1D theoretical calculation for $10T_L < t < 20T_L$ due to that some ions are being pushed away from the axis in the transverse direction and the remaining ions within the window are accelerated more efficiently by the radiation pressure. At later stages after $t = 20T_L$, the simulation shows a lower value of p_{ix} than the theoretical calculation due to the RTI-induced transparency. The evolution and broadening of the ion energy spectra within the window can be seen from Fig. 2(b). Significant broadening of the energy spectra with energy spread ratio ($\Delta E/E_p$) greater than 20%, where ΔE is the full width half maximum energy spread and E_p is the average energy of the trapped ions, occurs around $t = 16T_L$. In Fig. 2(c), the evolution of the normalized average electron density within a $0.05\lambda_L \times 4\lambda_L$ window co-moving with the target (the line with initial value 1.7) shows that the radiation pressure initially compresses the electron layer to a state with higher density (greater than 3 times the initial density), and then the RTI starts to broaden the foil and decrease the electron density. After $t = 16T_L$, the normalized average electron density $n_e/(n_c a_0)$ drops below 1, which indicates that the electron density is below the relativistic critical density, and the foil becomes transparent to the laser light. This can be further inferred from the evolution of the normalized average electron gamma factors (γ_e/a_0 , $\gamma_{e\parallel}/a_0$, and $\gamma_{e\perp}/a_0$) within the window in Fig. 2(c). During the RPA, as the electron layer density decreases due to the RTI, the laser light penetrates deeper into the electron layer and the transverse kinetic energy of the electrons within the laser penetration depth will become

ultra-relativistic, so that $\gamma_{e\perp} \sim a_0$. Therefore, the normalized average electron gamma factor $\gamma_{e\perp}/a_0$ grows larger as the laser light penetrates deeper and when the laser light fully penetrates the foil, we have $\gamma_{e\perp}/a_0 \approx 1$ occurring around $t = 16.5T_L$. At a later stage, the electron parallel velocity continues to grow as shown by $\gamma_{e\parallel}/a_0$ due to the development of the filamentation instability after the laser penetrating into the underdense plasma. We also note that during the RPA, the ion layer is compressed into a high energy density state as shown in Fig. 2(d). The energy density of the proton layer can be as high as $u_0 \sim 10^{17} \text{J/m}^3$.

To explore the scaling of the maximal obtainable energy of monoenergetic ions as a function of the incident laser power, we defined a quasi-monoenergetic ion beam as having an energy spread ratio $\Delta E/E_p$ below 20% and performed two sets of 2D PIC simulations, one for the RPA of protons and the other for carbon ions. In the simulations, the foil density is chosen to scale linearly with the normalized incident laser amplitude a_0 , so that the foil thickness is fixed to be $l_0 = 0.2\lambda_L$, satisfying the optimal thickness condition described in Eq. (1). Figure 3 shows the maximal quasi-monoenergetic ion energy vs the incident laser amplitude along with the occurrence time of the maximum energy, t_s . Here, the maximal quasi-monoenergetic ion energy is almost proportional to a_0 with a nearly constant t_s/T_L (15.8 ± 1.7 and 12.9 ± 1.4 for protons and carbon ions, respectively).

III. DISCUSSION ON THE ENERGY SCALING

To explain the weak dependence of t_s on laser power in the RPA, we apply the theory of mode growth of the RTI. First, we estimate the required density reduction for the

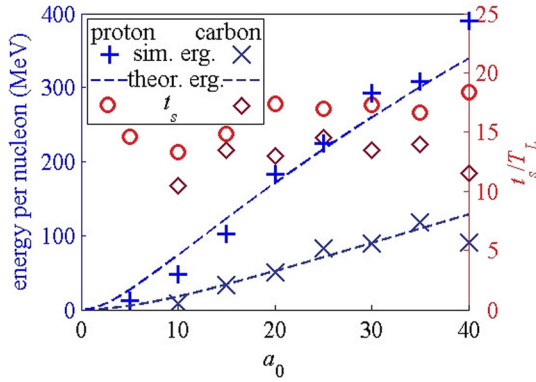


FIG. 3. (Color online) The energy scaling from 2D PIC simulations for protons and carbon ions. The saturation time t_s is recorded when the maximum of quasi-monoenergy (under the constraint $\Delta E/E_p \leq 20\%$) is obtained. The dashed lines are theoretical calculations of the energy scaling.

occurrence of underdense condition which can induce the broadening of the proton energy spectrum. In our simulation, the foil thickness is fixed to be $l_0 = 0.2\lambda_L$, and thus the initial density in the target is related to the critical density through $n_0 = (a_0/\pi)(\lambda_L/l_0)n_c = 1.6a_0n_c$. Relativistic underdense condition $\varepsilon = 1 - n_e/(a_0n_c) > 0$ is met when the density drops to satisfy $n_e < a_0n_c = n_0/1.6$. Therefore, the density reduction factor for the underdense condition $n_e(t_s)/n_0 = 1/1.6$ is a constant independent of a_0 in our simulations.

Figures 4(a) and 4(b) show the simulated transverse distribution of average ion density at three instants for two different laser intensities, indicating the occurrence of mode growth of the RTI. For the higher laser intensity $a_0 = 25$ [Fig. 4(b)], the ion density develops periodic structures with a periodicity comparable to the laser wavelength, whereas for $a_0 = 5$ [Fig. 4(a)], the structures have shorter periodicity. The growth rate of the RTI is proportional to \sqrt{gk} for a

mode of characteristic transverse wave number k , where g is the acceleration. We define the total RTI growth factor as $\alpha = \sqrt{k_s} \int_0^{t_s} \sqrt{g(t)} dt$ to represent the exponential growth of the density fluctuation amplitude, where $2\pi/k_s$ is the dominant transverse periodic structure scale length appearing just before the broadening of the proton energy spectrum and can be obtained from the simulation. The acceleration $g(t) = d(\gamma v)/dt$ can be obtained from Eq. (2). This factor α at the saturation time $t = t_s$ for different input laser amplitudes a_0 are calculated from our simulations.

Figure 4(c) shows that the dependence of the calculated total growth factor α on the laser amplitude a_0 , indicating that the growth factor is nearly independent of the laser amplitude a_0 . To explain this, we can explore the dependence of the contributing factors $\int_0^{t_s} \sqrt{g(t)} dt$ and k_s to α on a_0 . Figure 4(d) shows that the factor $\int_0^{t_s} \sqrt{g(t)} dt$ increases with a_0 but is flattened for large a_0 . For $a_0 > 20$, the Doppler effect of the laser radiation as shown in Eq. (2) limits the acceleration and consequently determines the weak dependence of the growth factor on laser amplitude. From the dependence of the saturation wave number on a_0 shown in Fig. 4(d), it can be seen that for a laser amplitude $a_0 < 10$, the transverse periodic structure has a dominant scale length less than λ_L , which is due to that smaller length-scale structures grow faster and the RTI did not yet reach saturation when the induced transparency occurs. For laser amplitudes $a_0 > 20$, the transverse periodic structures have scale lengths approximately equal to λ_L , the saturation length scale for the RTI. Combining the opposite dependence of $\int_0^{t_s} \sqrt{g(t)} dt$ and k_s on a_0 , we can explain the growth factor α thus obtained is nearly independent of the laser amplitude a_0 .

Therefore, given that both the growth factor α and the density reduction factor for reaching the underdense

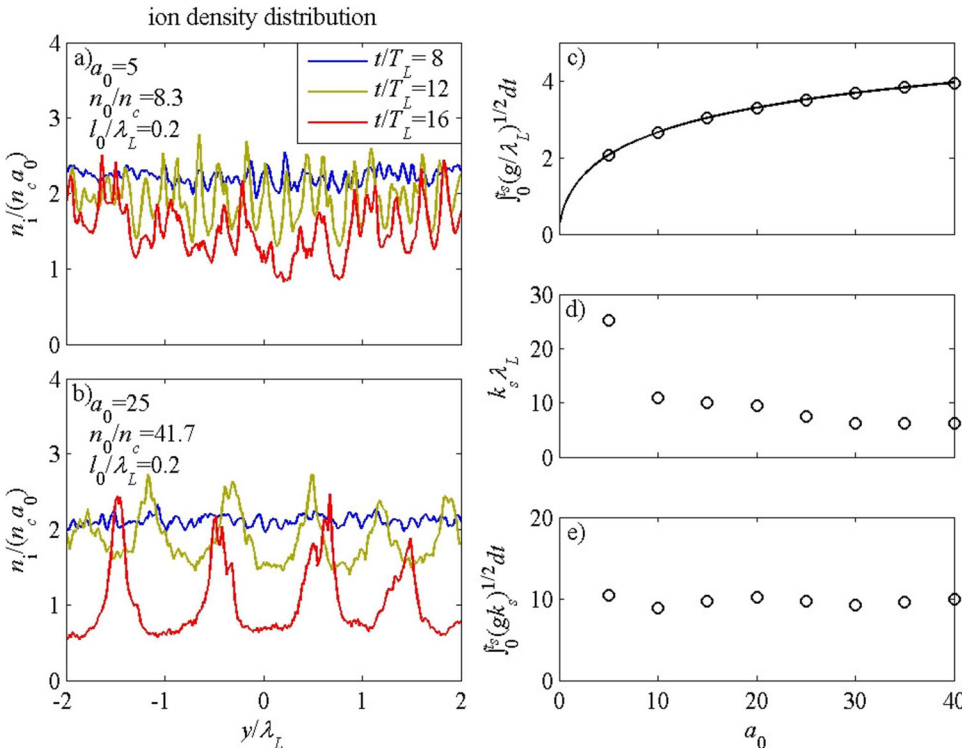


FIG. 4. (Color online) (a) The transverse ion density distribution averaged over a window along the laser propagation direction with the normalized laser wave amplitude $a_0 = 5$ and $n_0/n_c = 8.3$ at $t = 8T_L$, $t = 12T_L$, and $t = 16T_L$. (b) The case of incident laser amplitude $a_0 = 25$ and target density $n_0/n_c = 41.7$ at the same time instants as in (a). (c) The dependence of the total growth α of the mode with wave number k_s at the saturation time on the laser amplitude. (d) Values of $\int_0^{t_s} (g/\lambda_L)^{1/2} dt$ vs. normalized laser amplitude a_0 . (e) $k_s \lambda_L$ vs. a_0 , where $2\pi/k_s$ is the dominant transverse periodic structure scale length just before the broadening of the proton energy spectrum in the simulation.

condition are nearly independent of the laser amplitude a_0 , we can therefore explain the weak dependence of the quasi-monoenergetic ion beam development time t_s on the laser amplitude a_0 .

Assuming that t_s is independent of a_0 , we derive the energy scaling using the analytical solutions of Eq. (2)^{21,22} and obtain

$$E_{\text{quasi-mono}} = \frac{(\psi - 1)^2}{2\psi} m_i c^2, \quad (3)$$

where

$$\psi = 2 \sinh \left[\sinh^{-1} \left(2 + 6a_0^2 \frac{m_e n_c \lambda_L t_s}{m_i n_0 l_0 T_L} \right) / 3 \right]. \quad (4)$$

By further applying the optimal thickness condition, Eq. (1), we have

$$E_{\text{non-rel}} \approx 2 \left(\pi a_0 \frac{m_e t_s}{m_i T_L} \right)^2 m_i c^2 \quad (5)$$

for $\pi a_0 t_s / T_L \ll m_i / m_e$ and

$$E_{\text{ultra-rel}} \approx \left(\frac{3}{2} \pi a_0 \frac{m_e t_s}{m_i T_L} \right)^{1/3} m_i c^2 \quad (6)$$

for $\pi a_0 t_s / T_L \gg m_i / m_e$, consistent with the results derived from previous works.^{10,21,22,25} The scaling of the quasi-monoenergetic ion energy thus calculated is shown as dashed lines in Fig. 3, where $6n_{C0} = n_{p0} = n_{e0}$ and $m_C = 12m_p = 12 \times 1836m_e$ are applied, and agrees well with the simulation results for the RPA of both protons and carbon ions. Here, t_s is chosen to be $18T_L$ for protons and $14T_L$ for carbon

ions, slightly longer than those from the simulations to compensate the loss of ions off the axis during the acceleration in the 2D simulation. Equation (3) also shows that, since $n_{C0} m_C = 2n_{p0} m_p$, the acceleration of the carbon foil is half that of the proton foil, indicating that the average energy of carbon ions is then 3 times that of proton ions at the same time since $m_C v_C^2 / 2 = (12m_p)(v_p/2)^2 / 2 = 3m_p v_p^2 / 2$. The scaling suggests that for a flat ultra-thin target of optimal thickness, the quasi-monoenergetic proton and carbon ion energy can reach about 200 MeV and 100 MeV per nucleon, respectively, with $a_0 = 25$, corresponding to around 1 PW laser power. This opens up the possibility of applying RPA-based laser hadron accelerator with sub-petawatt laser for medical applications, fast ignition, and proton imaging methods.

IV. THE INFLUENCE OF DIFFERENT INITIAL CONDITIONS ON THE RESULTS

The scaling in Fig. 3 shows that although the development time t_s is independent of input amplitude a_0 , the accelerating times for proton and carbon ion cases are slightly different. To investigate the dependence of t_s on different initial conditions and to verify that the mechanism of the RPA is still the same among different input parameters, we compare the evolution results with the cases of a laser beam with plane wave profile in transverse dimension and a thinner foil target.

Figure 5 shows the evolution of particles at the same time steps as in Fig. 1, while we use circularly polarized plane wave instead of Gaussian beam to illuminate on the foil. The interleaving high and low density regions in transverse dimension indicate that RTI is still the principal instability in destroying the electron layer and broadening the

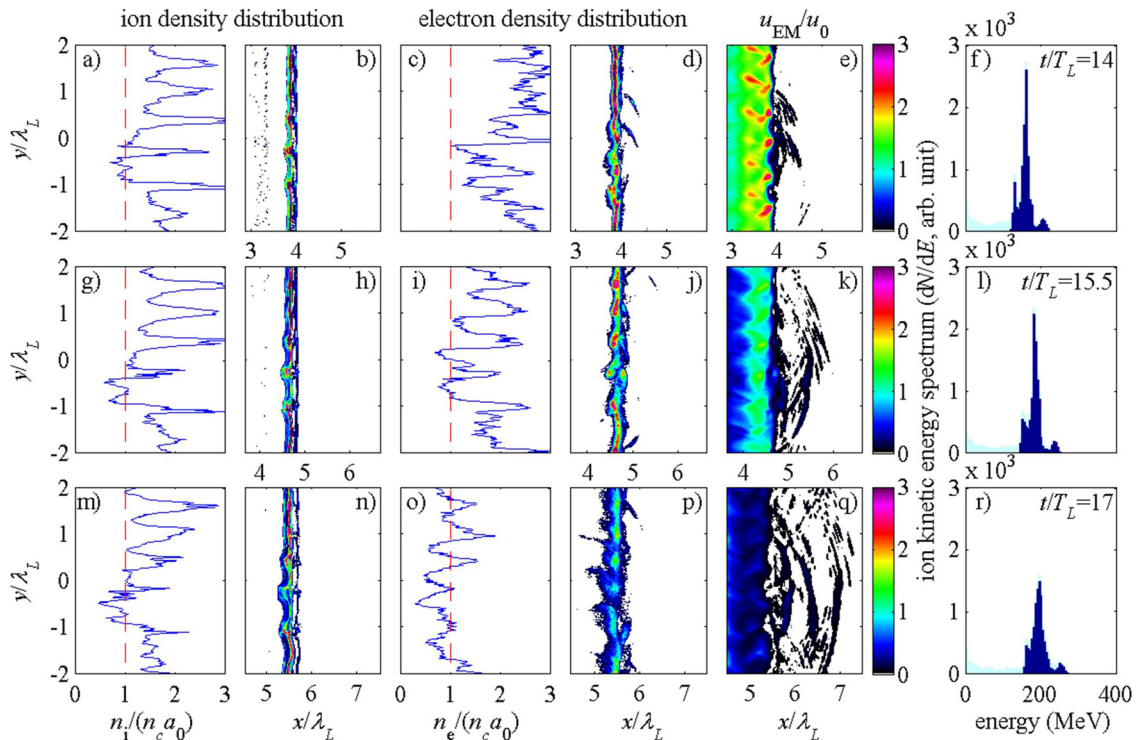


FIG. 5. (Color online) The same simulation as in Fig. 1 but the Gaussian beam is replaced by a plane wave.

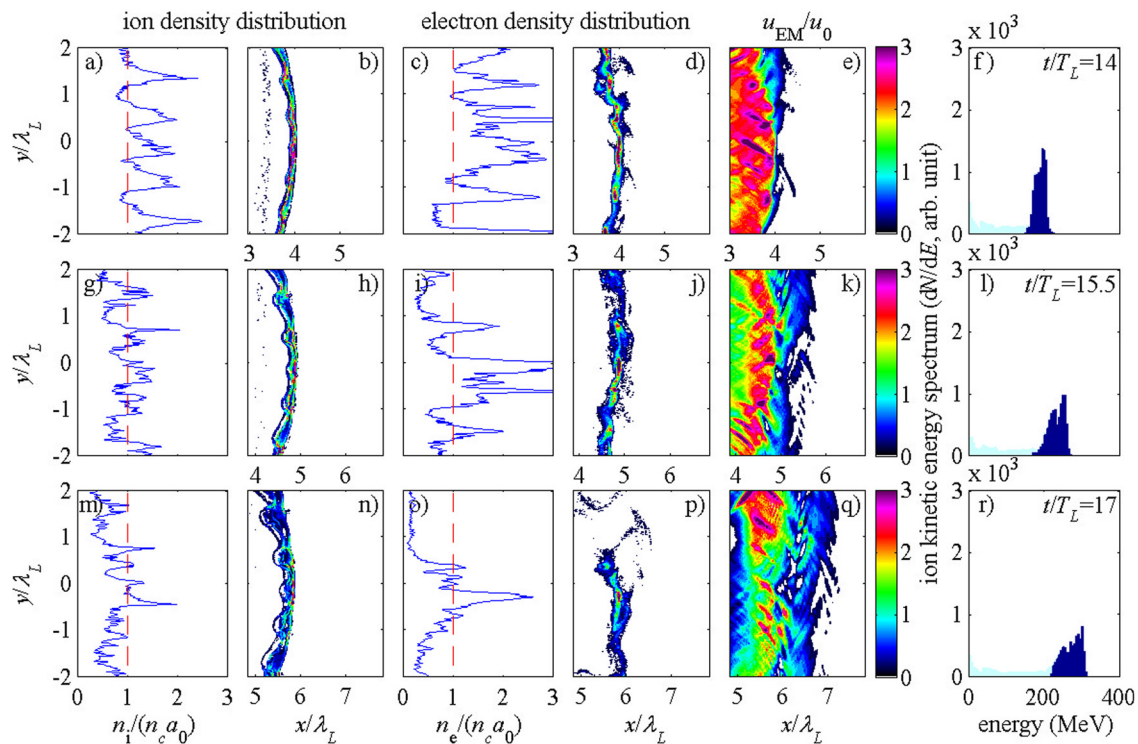


FIG. 6. (Color online) The same simulation as in Fig. 1 but the foil density is doubled and thickness is halved.

energy spectrum. The time of transparency $t_s = 18T_L$ is longer than the Gaussian beam case by about 1.5 wave periods due to a slower density reducing speed, and the similar average energies with the Gaussian beam case verifies the RPA mechanism and the validity of Eqs. (3) and (4). Since the spot size of the Gaussian profile is large compared to the foil thickness and the laser wavelength, the foil development in the center part does not differ from the plane wave case considerably, hence the differences in t_s between these two cases are not so significant.

Figure 6 shows the same plots while we decrease the thickness of the foil to $l_0 = 0.1 \lambda_L$ and consequently increase the density $n_0 = 83.3n_c$ to keep Eq. (1) satisfied. The average energy is also the same and agrees with Eqs. (3) and (4) and the developing time $t_s = 14.5T_L$ is $2T_L$ less than the original case, that is, the energy spread at $17T_L$ is $\Delta E/E = 22.8\%$, slightly greater than the case of thicker foil, since initially when electrons are pushed forward, a denser proton foil has a greater relative initial density perturbation and Coulomb repulsion force. The similarity between these two cases shows that the scaling law within the range of moderately altered density and thickness is still valid with marginally modified t_s values. Further study will be performed for density close to real foils.

V. CONCLUSIONS

In summary, we have reported here the energy scaling of accelerated protons and carbon ions with laser radiation intensity for the laser radiation pressure acceleration of thin foils. We found that with a laser power of about one petawatt, quasi monogenic protons with 200 MeV and carbon ions with 100 MeV per nucleon can be obtained. The limit of

energy is due to that light leaks through the foil caused by self-induced transparency at the density minima at the non-linear stage of the Raleigh-Taylor instability.

- ¹S. P. D. Mangles, C. D. Murphy, Z. Najmudin, A. G. R. Thomas, J. L. Collier, A. E. Dangor, E. J. Divall, P. S. Foster, J. G. Gallacher, C. J. Hooker, D. A. Jaroszynski, A. J. Langley, W. B. Mori, P. A. Norreys, F. S. Tsung, R. Viskup, B. R. Walton, and K. Krushelnick, *Nature* **431**, 535 (2004); C. G. R. Geddes, Cs. Toth, J. van Tilborg, E. Esarey, C. B. Schroeder, D. Bruhwiler, C. Nieter, J. Cary, and W. P. Leemans, *Nature* **431**, 538 (2004); J. Faure, Y. Glinec, A. Pukhov, S. Kiselev, S. Gordienko, E. Lefebvre, J.-P. Rousseau, F. Burgy, and V. Malka, *Nature* **431**, 541 (2004).
- ²W. P. Leemans, B. Nagler, A. J. Gonsalves, Cs. Tóth, K. Nakamura, C. G. R. Geddes, E. Esarey, C. B. Schroeder, and S. M. Hooker, *Nat. Phys.* **2**, 696 (2006).
- ³K. W. D. Ledingham, W. Galster, and R. Sauerbrey, *Br. J. Radiol.* **80**, 855 (2007).
- ⁴M. Roth, T. E. Cowan, M. H. Key, S. P. Hatchett, C. Brown, W. Fountain, J. Johnson, D. M. Pennington, R. A. Snavely, S. C. Wilks, K. Yasuike, H. Ruhl, F. Pegoraro, S. V. Bulanov, E. M. Campbell, M. D. Perry, and H. Powell, *Phys. Rev. Lett.* **86**, 436 (2001).
- ⁵J. J. Honrubia, J. C. Fernández, M. Temporal, B. M. Hegelich, and J. Meyer-ter-Vehn, *Phys. Plasmas* **16**, 102701 (2009).
- ⁶J. A. Cobble, R. P. Johnson, T. E. Cowan, N. Renard-Le Galloudec, and M. Allen, *J. Appl. Phys.* **92**, 1775 (2002).
- ⁷M. Borghesi, A. Schiavi, D. H. Campbell, M. G. Haines, O. Willi, A. J. MacKinnon, L. A. Gizzi, M. Galimberti, R. J. Clarke, and H. Ruhl, *Plasma Phys. Control. Fusion* **43**, A267 (2001).
- ⁸S. C. Wilks, A. B. Langdon, T. E. Cowan, M. Roth, M. Singh, S. Hatchett, M. H. Key, D. Pennington, A. MacKinnon, and R. A. Snavely, *Phys. Plasmas* **8**, 542 (2001).
- ⁹A. Pukhov, *Phys. Rev. Lett.* **86**, 3562 (2001).
- ¹⁰T. Esirkepov, M. Borghesi, S. V. Bulanov, G. Mourou, and T. Tajima, *Phys. Rev. Lett.* **92**, 175003 (2004).
- ¹¹B. M. Hegelich, B. J. Albright, J. Cobble, K. Flippo, S. Letzring, M. Paffett, H. Ruhl, J. Schreiber, R. K. Schulze, and J. C. Fernández, *Nature* **439**, 441 (2006).
- ¹²H. Schwöerer, S. Pfotenhauer, O. Jäckel, K.-U. Amthor, B. Liesfeld, W. Ziegler, R. Sauerbrey, K. W. D. Ledingham, and T. Esirkepov, *Nature* **439**, 445 (2006).

- ¹³S. Ter-Avetisyan, M. Schnürer, P. V. Nickles, M. Kalashnikov, E. Risse, T. Sokollik, W. Sandner, A. Andreev, and V. Tikhonchuk, *Phys. Rev. Lett.* **96**, 145006 (2006).
- ¹⁴J. Fuchs, C. A. Cecchetti, M. Borghesi, T. Grismayer, E. d'Humières, P. Antici, S. Atzeni, P. Mora, A. Pipahl, L. Romagnani, A. Schiavi, Y. Sentoku, T. Toncian, P. Audebert, and O. Willi, *Phys. Rev. Lett.* **99**, 015002 (2007).
- ¹⁵P. Mora, *AIP Conf. Proc.* **920**, 98 (2007).
- ¹⁶L. Robson, P. T. Simpson, R. J. Clarke, K. W. D. Ledingham, F. Lindau, O. Lundh, T. McCanny, P. Mora, D. Neely, C.-G. Wahlström, M. Zepf, and P. McKenna, *Nat. Phys.* **3**, 58 (2007).
- ¹⁷<http://meetings.aps.org/link/BAPS.2009.DPP.GO6.3>. This abstract shows that proton energies in excess of 65 MeV was obtained from the experiment in Los Alamos National Laboratory.
- ¹⁸X. Q. Yan, C. Lin, Z. M. Sheng, Z. Y. Guo, B. C. Liu, Y. R. Lu, J. X. Fang, and J. E. Chen, *Phys. Rev. Lett.* **100**, 135003 (2008).
- ¹⁹C. S. Liu, V. K. Tripathi, and X. Shao, *AIP Conf. Proc.* **1061**, 246 (2008).
- ²⁰O. Klimo, J. Psikal, J. Limpouch, and V. T. Tikhonchuk, *Phys. Rev. ST Accel. Beams* **11**, 031301 (2008).
- ²¹A. P. L. Robinson, M. Zepf, S. Kar, R. G. Evans, and C. Bellei, *New J. Phys.* **10**, 013021 (2008).
- ²²V. K. Tripathi, C. S. Liu, X. Shao, B. Eliasson, and R. Z. Sagdeev, *Plasma Phys. Control. Fusion* **51**, 024014 (2009).
- ²³B. Eliasson, C. S. Liu, X. Shao, R. Z. Sagdeev, and P. K. Shukla, *New J. Phys.* **11**, 073006 (2009).
- ²⁴T. P. Yu, A. Pukhov, G. Shvets, and M. Chen, *Phys. Rev. Lett.* **105**, 065002 (2010).
- ²⁵T. P. Yu, A. Pukhov, G. Shvets, M. Chen, T. H. Ratliff, S. A. Yi, and V. Khudik, *Phys. Plasmas* **18**, 043110 (2011).
- ²⁶M. Chen, N. Kumar, A. Pukhov, and T. P. Yu, *Phys. Plasmas* **18**, 073106 (2011).
- ²⁷B. Qiao, M. Zepf, M. Borghesi, and M. Geissler, *Phys. Rev. Lett.* **102**, 145002 (2009).
- ²⁸M. Chen, A. Pukhov, and T. P. Yu, *Phys. Rev. Lett.* **103**, 024801 (2009).
- ²⁹A. Henig, D. Kiefer, K. Markey, D. C. Gautier, K. A. Flippo, S. Letzring, R. P. Johnson, T. Shimada, L. Yin, B. J. Albright, K. J. Bowers, J. C. Fernández, S. G. Rykovanov, H.-C. Wu, M. Zepf, D. Jung, V. Kh. Liechtenstein, J. Schreiber, D. Habs, and B. M. Hegelich, *Phys. Rev. Lett.* **103**, 045002 (2009).
- ³⁰F. Pegoraro and S. V. Bulanov, *Phys. Rev. Lett.* **99**, 065002 (2007).
- ³¹J. P. Verboncoeur, A. B. Langdon, and N. T. Gladd, *Comput. Phys. Commun.* **87**, 199 (1995).